QUARTERLY JOURNAL OF THE ROYAL METEOROLOGICAL SOCIETY
Q. J. R. Meteorol. Soc. **135**: 1277–1291 (2009)
Published online 3 June 2009 in Wiley InterScience
(www.interscience.wiley.com) DOI: 10.1002/qj.431

Interactions between dry-air entrainment, surface evaporation and convective boundary-layer development

Chiel C. van Heerwaarden*, Jordi Vilà-Guerau de Arellano, Arnold F. Moene and Albert A. M. Holtslag

Meteorology and Air Quality Section, Wageningen University, The Netherlands

ABSTRACT: The influence of dry-air entrainment on surface heat fluxes and the convective boundary-layer (CBL) properties is studied for vegetated land surfaces, using a mixed-layer CBL model coupled to the Penman–Monteith equation under a wide range of conditions. In order to address the complex behaviour of the system, the feedback mechanisms involved were put into a mathematical framework. Simple expressions for the evaporative fraction and the Priestley–Taylor parameter were derived, based on the concept of equilibrium evaporation. Dry-air entrainment enhances the surface evaporation under all conditions, but the sensitivity of the evaporation rate to the moisture content of the free troposphere falls as temperature rises. Due to the evaporation enhancement, shallower CBLs develop beneath dry atmospheres. In all cases, dry-air entrainment reduces the relative humidity at the land surface and at the top of the CBL. However, because of dry-air entrainment-induced land–atmosphere feedback mechanisms, relative humidity at the top of the CBL responds nonlinearly to temperature rise; it decreases as temperature rises beneath a moist free troposphere, whereas it increases beneath a dry free troposphere. Finally, it was found that in certain conditions the evolution of the surface fluxes, relative humidity and CBL height can be as sensitive to the free tropospheric moisture conditions as to the land-surface properties. Therefore, studies of the land surface and of convective clouds have to take into account the influence of dry-air entrainment through land–atmosphere feedback mechanisms. Copyright © 2009 Royal Meteorological Society

KEY WORDS surface heat fluxes; land–atmosphere interactions

Received 27 January 2009; Revised 20 April 2009; Accepted 20 April 2009

1. Introduction

The convective boundary layer (CBL) over land is closely coupled to the land surface and the free troposphere (e.g. de Bruin, 1983; Jacobs and de Bruin, 1992; Betts, 2004). Its evolution throughout the day largely depends on the partitioning of the available energy into latent and sensible heat fluxes at the land surface. The latent heat flux moistens the CBL, while the sensible heat flux provides the energy that induces CBL growth and the entrainment of free-tropospheric air into the CBL. Due to the coupled nature of the land–atmosphere system, the CBL feeds back to the partitioning of the surface heat fluxes by modifying the atmospheric demand for water. In other words, the CBL regulates how intensely the atmosphere can extract water from the land surface.

In this system, in which the land surface, the CBL and the free troposphere interact, surface energy partitioning evolves towards a state that is known as equilibrium evaporation (Priestley and Taylor, 1972), when the evaporative fraction, $EF(= LE/(H + LE)$, in which H is the sensible and LE the latent heat flux) reaches a steady state, because the atmospheric demand for water has become constant (Raupach, 1991, 2000). In this state the extra water capacity of the CBL that is induced by heating is exactly compensated for by an increase in the atmospheric moisture content. In the absence of large-scale advection, two processes determine CBL moisture content: evaporation at the land surface and entrainment of dry air at the interface of the CBL and the free troposphere.

In this paper we focus on the complex role of dry-air entrainment in the CBL evolution over vegetated land surfaces. The first effect of dry-air entrainment is simple, namely, a reduction in the specific humidity of the CBL. Subsequently, a set of feedback mechanisms is triggered, leading to complex interactions between the land surface and the atmosphere. The latent heat flux increases beneath a drier atmosphere, but this immediately implies a reduction of the sensible heat flux that results in reduced CBL growth and therefore less dry-air entrainment.

Due to these feedback mechanisms, it is not clear whether dry-air entrainment can systematically enhance the equilibrium evaporation. The first indirect indication that it might do so originated from the work of Priestley and Taylor (1972). Their analysis of daily evaporation rates over wet surfaces showed that the EF was approximately 1.26 times the value of the equilibrium EF, but

*Correspondence to: C. C. van Heerwaarden, Meteorology and Air Quality Section, Wageningen University, PO Box 47, 6700 AA Wageningen, The Netherlands.
E-mail: chiel.vanheerwaarden@wur.nl

they based their equilibrium expression on a CBL of constant height, being unaware of the effects of entrainment. Priestley and Taylor (1972) therefore did not relate the increase of EF to dry-air entrainment. The first to link the two were de Bruin (1983) and McNaughton and Spriggs (1986), who were able to reproduce the EF enhancement by including dry-air entrainment into a conceptual model that coupled the land surface to the CBL. Later, Culf (1994) and Betts (1994) derived an analytical expression for equilibrium evaporation including entrainment. By applying typical values for CBL properties in their expression, they showed that the increase in the EF by entrainment corresponds to the findings of Priestley and Taylor (1972). Although equilibrium evaporation over wet surfaces is enhanced by dry-air entrainment, none of the papers discussed whether any enhancement occurs over dry surfaces characterised by low soil moisture. Raupach (2000) has raised some doubts about the use of equilibrium evaporation in dry conditions, suggesting that under these conditions convergence to equilibrium evaporation cannot be achieved on a semi-diurnal time-scale. This is because the characteristic time-scale of the system largely increases under dry conditions, due to the large surface resistance and deep CBLs.

In this study, we systematically investigate the influence of dry-air entrainment on the partitioning of the surface heat fluxes and their propagation into the properties of the CBL through the land-surface feedbacks for a large and complete range of atmospheric and land-surface conditions. Our methodology is based on a coupled land–atmosphere model similar to that of McNaughton and Spriggs (1986), consisting of a slab model for the CBL (Tennekes, 1981) and the Penman–Monteith equation (Monteith, 1965) to solve the surface energy balance. This methodology has proven to be an adequate tool for dealing with the essential dynamics of a growing CBL coupled to the land surface (e.g. de Bruin, 1983; McNaughton and Spriggs, 1986; Raupach, 2000, 2001; Freedman *et al.*, 2001).

The first aim of this paper is to quantify the role of dry-air entrainment on the partitioning of surface heat fluxes. First, we explain in section 2 the physical feedback mechanisms in the CBL that direct the system towards equilibrium evaporation. We derive a new and simple expression of equilibrium evaporation based on the slab equations of the CBL and we validate this expression against the coupled model. In section 3 we introduce the model and the experiments that we perform. Next, in section 4.1, we perform an analysis on the sensitivity of the equilibrium EF to the moisture conditions in the free troposphere and evaluate the use of the concept of equilibrium evaporation for both wet and dry surfaces.

Our second aim is to study how strongly dry-air entrainment feeds back to the CBL structure. In order to demonstrate the feedback mechanisms involved, we first explore in section 4.3 the semi-diurnal evolution of the CBL in a typical case for which we perturb the state of the free-tropospheric moisture. Subsequently, in section 4.4.1, we perform multiple series of numerical experiments to analyse the sensitivity of the surface fluxes, the CBL height and the relative humidity (RH) at the land surface and the CBL top to a range of free-tropospheric conditions. We chose to analyse these variables on the basis of their importance for studies concerning air quality, the water balance and cloud formation. Finally, in section 4.4.3 we simulate an ensemble of model runs for a range of free-tropospheric moisture and land-surface conditions in order to study the relevance of the free troposphere vis-à-vis the the land-surface conditions in the determination of EF and the CBL properties. By doing so, we show that the influence of the free-tropospheric moisture on the partitioning of the surface heat fluxes and the CBL evolution has generally been underestimated by many modelling studies that regard land-surface conditions and atmospheric stability as the dominant factors in the evolution of surface heat fluxes and the state of the CBL (e.g. de Bruin, 1983; Santanello *et al.*, 2007; Trier *et al.*, 2008).

2. Equilibrium evaporation beneath a growing CBL

2.1. Relevance of the concept

In this study we use the concept of equilibrium evaporation to improve our understanding of the effects of dry-air entrainment on evaporation. This concept allows us to relate the surface processes to all the processes that occur in the CBL and to understand their connected behaviour. We learned from previous studies (McNaughton and Spriggs, 1986; Culf, 1994; Betts, 1994; Raupach, 2000, 2001) that the CBL drives the surface fluxes towards a state in which the atmospheric demand for water becomes constant. If we wish to describe the partitioning of the surface fluxes in this state and whether it can be achieved, we need to understand and quantify the feedback mechanisms that drive the process of regulation.

2.2. Feedback mechanisms in the coupled land–atmosphere system

Here, we discuss the mechanisms that regulate the heat exchange between the land surface and the CBL. Since there is a set of negative feedback mechanisms that regulates evaporation, there is only one stable equilibrium for the evaporation rate. Figure 1 is a diagram of the negative feedback mechanisms and the relationships among the variables involved in them. In short, they are:

- Feedback 1 is the *heating* feedback (dashed line). This mechanism enhances evaporation when the atmosphere warms up. The excess available energy that is not used for evaporation (LE) is released as sensible heat H. This flux directly increases the CBL potential temperature θ (feedback 1.1) and through entrainment of heat at the top of the CBL, h (feedback 1.2). In consequence, the atmospheric demand for water rises. LE is therefore enhanced, while H falls.

DOI: 10.1002/qj

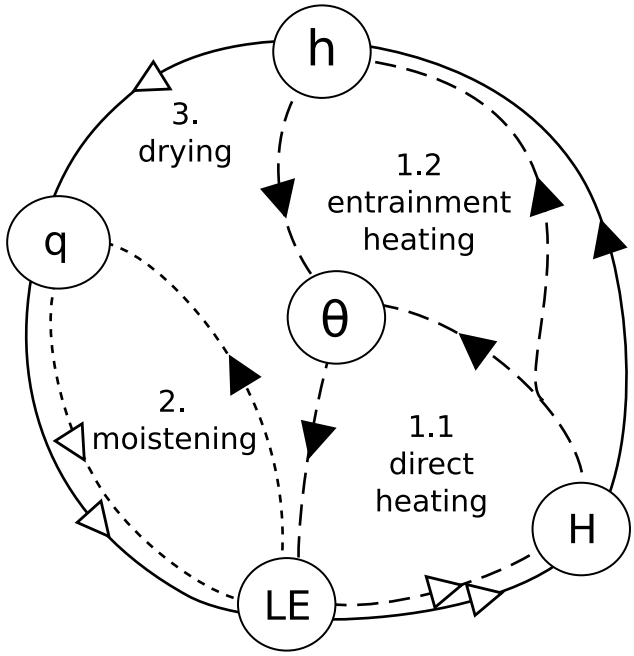

Figure 1. Feedbacks in the coupled land–atmosphere system. Closed arrows represent positive relationships, and open arrows negative relationships. Each of the three feedbacks has a distinct line style. LE is the latent heat flux, H is the sensible heat flux, θ is the bulk potential temperature of the CBL, q is the bulk specific humidity of the CBL and h is the CBL height.

- Feedback 2 is the *moistening* feedback (dotted line). This mechanism reduces evaporation when the atmosphere becomes more humid. The diagram shows that evaporation LE leads to a higher specific humidity q. Consequently, the gradient of specific humidity between the land surface and the CBL decreases and LE is reduced.
- Feedback 3 is the *drying* feedback (solid line) that enhances evaporation when the CBL becomes drier. This feedback is similar to the heating feedback, driven by the sensible heat flux H, which triggers CBL growth (increasing h) through the entrainment process. As the CBL grows, dry free-tropospheric air is entrained into the boundary layer and the specific humidity of the CBL, q, therefore decreases. This results in an increase of LE and a fall in H. Usually this feedback is negative as a decrease in LE is opposed, but in the rare event that the free-tropospheric air contains more moisture than the CBL, the feedback can become positive.

Later in this study, we make extensive use of the diagram to explain the behaviour of the coupled land–atmosphere system under various conditions.

2.3. Feedbacks in a mathematical framework

In this section we put the concept of equilibrium evaporation into a mathematical framework that enables us to quantify the importance of entrainment. In equilibrium, the CBL's demand for water ($q_{\mathrm{sat}} - q$) is constant and therefore air from the CBL that is adiabatically transported to the land surface must fulfill the following condition (Culf, 1994):

$$\left.\frac{\mathrm{d}q_{\mathrm{sat}}}{\mathrm{d}T}\right|_T \frac{\mathrm{d}T}{\mathrm{d}t} - \frac{\mathrm{d}q}{\mathrm{d}t} = 0, \tag{1}$$

in which $\mathrm{d}q_{\mathrm{sat}}/\mathrm{d}T$ is the slope of the saturated specific humidity evaluated at the air temperature, T is the air temperature and q is the specific humidity. McNaughton and Spriggs (1986) pointed out that this state is a quasi-equilibrium as it depends on temperature. However, the use of this equilibrium was validated by Raupach (2000), who showed that the rate of change of temperature with time is slow compared to the characteristic time-scales of the feedbacks under wet to moderately dry conditions.

By assuming that the temperature T equals the potential temperature θ at the land surface, Raupach (2000) showed that the above relationship can be rewritten in a form that is valid at all heights within the CBL by deriving the so-called potential saturation deficit $q_{\mathrm{sat}}(\theta) - q$ in time. This yields an equation containing only conserved variables:

$$\left.\frac{\mathrm{d}q_{\mathrm{sat}}}{\mathrm{d}T}\right|_\theta \frac{\mathrm{d}\theta}{\mathrm{d}t} - \frac{\mathrm{d}q}{\mathrm{d}t} = 0, \tag{2}$$

in which $\mathrm{d}q_{\mathrm{sat}}/\mathrm{d}T$ is the slope of the saturated specific humidity evaluated at the potential temperature, θ. Hereafter, each instance of $\mathrm{d}q_{\mathrm{sat}}/\mathrm{d}T$ is evaluated at θ.

In our study we limit ourselves to a cloudless CBL, which implies that we can substitute the temperature and moisture tendencies in the previous equation by those proposed by the mixed-layer theory for the CBL (Tennekes, 1973, 1981) resulting in the following equation under equilibrium conditions:

$$\left.\frac{\mathrm{d}q_{\mathrm{sat}}}{\mathrm{d}T}\right|_\theta \frac{1}{h}\left\{\overline{w'\theta'}_{\mathrm{s}} + w_{\mathrm{e}}\Delta\theta\right\} - \frac{1}{h}\left\{\overline{w'q'}_{\mathrm{s}} + w_{\mathrm{e}}\Delta q\right\} = 0, \tag{3}$$

where $\overline{w'\theta'}_{\mathrm{s}}$ and $\overline{w'q'}_{\mathrm{s}}$ are the kinematic surface fluxes of potential temperature and specific humidity. Furthermore, h is the CBL height and $\Delta\theta$ and Δq are the jumps of potential temperature and specific humidity at the interface of the CBL and the free troposphere, defined as the free-tropospheric value minus the CBL value. The entrainment velocity w_{e} is parametrized as:

$$w_{\mathrm{e}} = A_{\theta_{\mathrm{v}}} \frac{\overline{w'\theta'_{\mathrm{v}}}_{\mathrm{s}}}{\Delta\theta_{\mathrm{v}}}, \tag{4}$$

in which $\overline{w'\theta'_{\mathrm{v}}}_{s}$ is the virtual potential temperature flux at the land surface, $A_{\theta_{\mathrm{v}}}$ is the ratio between the virtual potential temperature fluxes in the entrainment zone and at the land surface and $\Delta\theta_{\mathrm{v}}$ is the jump of virtual potential temperature at the interface of the CBL and the free troposphere.

DOI: 10.1002/qj

Rewriting the kinematic fluxes in terms of heat fluxes ($H = \rho c_p \overline{w'\theta'}_s$, $LE = \rho L_v \overline{w'q'}_s$) results in the following equation:

$$\overbrace{\frac{\mathrm{d}q_{\mathrm{sat}}}{\mathrm{d}T}\frac{H}{\rho c_p h}}^{\text{heating}} - \overbrace{\frac{LE}{\rho L_v h}}^{\text{moistening}} + \overbrace{\frac{\mathrm{d}q_{\mathrm{sat}}}{\mathrm{d}T} A_{\theta_v} \frac{\Delta\theta}{\Delta\theta_v}\left\{\frac{H}{\rho c_p h} + \theta\left(\frac{R_v}{R_d} - 1\right)\frac{LE}{\rho L_v h}\right\}}^{\text{entrainment heating}} - \overbrace{A_{\theta_v}\frac{\Delta q}{\Delta\theta_v}\left\{\frac{H}{\rho c_p h} + \theta\left(\frac{R_v}{R_d} - 1\right)\frac{LE}{\rho L_v h}\right\}}^{\text{drying}} = 0, \tag{5}$$

where H and LE are the surface sensible and latent heat flux, ρ the air density, c_p is the heat capacity of dry air, L_v the heat of vaporisation of water and R_v and R_d the gas constants of moist and dry air respectively.

In the equation we can identify the processes explained in Figure 1. The first term describes the direct heating of feedback 1.1, whereas heat entrainment (feedback 1.2) is expressed by term 2. Notice that the entrainment of heat is parametrized as a fixed fraction of the virtual heat flux at the surface, thus both H and LE enter in this term. The third term is the moistening of the CBL through evaporation (feedback 2) and the final term describes the effect of dry-air entrainment on q through feedback 3.

Since Equation (5) describes a linear relation between H and LE, it can be rewritten in terms of the evaporative fraction. This yields an expression for EF in equilibrium evaporation in which all of the feedback mechanisms are contained:

$$EF_{\mathrm{eq}} = \frac{LE}{H + LE} = \frac{\frac{\mathrm{d}q_{\mathrm{sat}}}{\mathrm{d}T} + \frac{\mathrm{d}q_{\mathrm{sat}}}{\mathrm{d}T}A_{\theta_v}\frac{\Delta\theta}{\Delta\theta_v} - A_{\theta_v}\frac{\Delta q}{\Delta\theta_v}}{\frac{\mathrm{d}q_{\mathrm{sat}}}{\mathrm{d}T} + \frac{\mathrm{d}q_{\mathrm{sat}}}{\mathrm{d}T}c_0 A_{\theta_v}\frac{\Delta\theta}{\Delta\theta_v} - c_0 A_{\theta_v}\frac{\Delta q}{\Delta\theta_v} + \frac{c_p}{L_v}}, \tag{6}$$

$$\text{with} \quad c_0 = \left\{1 - \frac{c_p}{L_v}\theta_{\mathrm{ref}}\left(\frac{R_v}{R_d} - 1\right)\right\} = 0.93. \tag{7}$$

As buoyancy is insensitive to temperature, we use a reference value of 290 K for θ_{ref} in the equilibrium expression. We can thus simplify our equation by defining the constant c_0. In section 4.4.1, we calculate the value of the equilibrium EF for a wide range of parameters and discuss the contribution of the feedbacks in detail.

In the introduction we mentioned that Culf (1994) also derived an expression for the equilibrium evaporation beneath a growing CBL. He followed a more general approach than we did, as the only assumption he made was parametrising the entrainment virtual heat flux as a fixed ratio of the surface flux. He derived his equilibrium expressions from the Bowen ratios at the land surface and the top of the CBL. However, by including the mixed-layer equations, our expression shows explicitly the contribution of each individual feedback to the equilibrium. We are aware that our mixed-layer approach, in contrast to that of Culf (1994), is less accurate in situations in which the inversion in the free troposphere is very weak, because in these conditions entrainment is underestimated if the interface between the CBL and the free troposphere is considered as being sharp (Sullivan, 1998). Nevertheless, vanZanten *et al.* (1999) and Pino *et al.* (2006) showed that, for a large range of conditions, our CBL model is accurate.

2.4. Physical expression of the Priestley–Taylor parameter

In the introduction we wrote that Priestley and Taylor (1972) were the first to find a systematic enhancement of the evaporative fraction compared to the equilibrium evaporative fraction over a non-growing CBL (EF_o). Priestley and Taylor (1972) included this enhancement in their widely used expression by including a parameter α. Its value was fitted according to their dataset of evaporation rates over wet surfaces:

$$EF_{\mathrm{PT}} = \alpha EF_o = \alpha \frac{\frac{\mathrm{d}q_{\mathrm{sat}}}{\mathrm{d}T}}{\frac{\mathrm{d}q_{\mathrm{sat}}}{\mathrm{d}T} + \frac{c_p}{L_v}}. \tag{8}$$

Since we derived a physical expression for the EF beneath a growing CBL, the ratio of Equations (6) and (8) is a physical expression for the Priestley–Taylor parameter α:

$$\alpha = \frac{EF_{\mathrm{eq}}}{EF_o} = \frac{\frac{\mathrm{d}q_{\mathrm{sat}}}{\mathrm{d}T} + \frac{\mathrm{d}q_{\mathrm{sat}}}{\mathrm{d}T}A_{\theta_v}\frac{\Delta\theta}{\Delta\theta_v} - A_{\theta_v}\frac{\Delta q}{\Delta\theta_v}}{\frac{\mathrm{d}q_{\mathrm{sat}}}{\mathrm{d}T} + \frac{\mathrm{d}q_{\mathrm{sat}}}{\mathrm{d}T}c_0 A_{\theta_v}\frac{\Delta\theta}{\Delta\theta_v} - c_0 A_{\theta_v}\frac{\Delta q}{\Delta\theta_v} + \frac{c_p}{L_v}} \frac{\frac{\mathrm{d}q_{\mathrm{sat}}}{\mathrm{d}T} + \frac{c_p}{L_v}}{\frac{\mathrm{d}q_{\mathrm{sat}}}{\mathrm{d}T}}. \tag{9}$$

Note that if we put A_{θ_v} to zero in Equation (6), the equilibrium simplifies to the one used in Equation (8) and α becomes equal to one. In section 4.4.1 we evaluate the value of α alongside the derived expressions for the equilibrium EF, in order to illustrate that α is a variable rather than a fixed parameter of the system.

3. Coupled mixed-layer model

3.1. Model description

We use a conceptual model to validate our derived expressions for equilibrium evaporation (Equation (6)) and the Priestley–Taylor parameter (Equation (9)) and for exploring the effects of dry-air entrainment on the properties of the CBL. It consists of a mixed-layer model (Tennekes, 1981) that solves the CBL properties (CBL

DOI: 10.1002/qj

model hereafter) and the Penman–Monteith equation (Monteith, 1965) to solve the surface heat fluxes. As our model is essentially similar to that of McNaughton and Spriggs (1986), we only briefly discuss the assumptions that are incorporated in these equations and deviations from their model. McNaughton and Spriggs (1986) give a full description.

Before describing the model assumptions, we would like to stress that this model describes the evolution of evaporation and the convergence to equilibrium evaporation during a single day. The absence of night-time processes and balancing radiative cooling requires that this model is initialized with early-morning temperature and moisture profiles each day it is run.

3.1.1. *The surface model*

At the surface we apply the Penman–Monteith equation to calculate the latent heat flux and the other terms of the surface energy balance. Our calculations incorporate the following assumptions:

- The net radiation Q_* is prescribed to the model and is the only source of energy. This implies that we do not take into account the radiative feedback of a warming surface. Raupach (2001) showed that this feedback needs to be taken into account when we explore the limits of the possible solutions, but in a coupled convective case this feedback can be neglected.
- The ground heat flux G is assumed to be 10% of the net radiation Q_*, which has been validated over grass by de Bruin and Holtslag (1982).
- The aerodynamic resistance r_a in the Penman–Monteith equation is taken to be a constant with a value of $50\,s^{-1}\,m$, as this value is relatively constant for convective cases over grassland. In order to relate it to the mixed-layer model, the surface-layer top is assumed to be at 10% of the CBL height. By fixing r_a we neglect surface-layer feedbacks, but Jacobs and de Bruin (1992) showed that these do not change the qualitative behaviour of the system and are of minor importance compared to the feedbacks between the land surface and the CBL.
- In the Penman–Monteith equation, it is implicitly assumed that the land surface has no heat capacity. The surface temperature is therefore a result rather than a forcing of the surface heat fluxes.
- As net radiation is specified and the ground heat flux is parametrized, the latent, but also the sensible heat flux directly follows from the Penman–Monteith equation.
- The stomatal resistance r_s is constant during diurnal cycles in this study. We consider a land surface covered with grass for which the resistance is largely a function of soil moisture.

3.1.2. *CBL model*

In the model we parametrize the CBL by means of a mixed-layer model. In brief, this model consists of five prognostic equations resolving the CBL height and the mixed-layer value and the interface jump of the potential temperature θ and the specific humidity q. The mixed-layer model assumes the following:

- The CBL is considered to be well-mixed. This implies that both the potential temperature and specific humidity are in quasi-steady state and that their respective flux profiles are therefore linear.
- The interface between the CBL and the free troposphere is sharp. Therefore, the entrainment zone has an infinitisimal thickness.
- Full prognostic equations for the jumps of potential temperature and specific humidity at the CBL–free-troposphere interface are solved. We do not assume the product of the CBL height and the jump of virtual potential temperature at the CBL–free-troposphere interface to be constant, as McNaughton and Spriggs (1986) did.
- The ratio between the virtual potential temperature flux at the CBL–free-troposphere interface and the flux at the land surface A_{θ_v} is fixed at 0.2, while the entrainment fluxes of other quantities are parametrized as functions of the entrainment velocity and the jump between the CBL and the free troposphere of the variable. Since the exact value of A_{θ_v} is uncertain (Conzemius and Fedorovich, 2006), we show the sensitivity of the results to the value of this variable in section 4.4.2.

3.2. Numerical experiments

Here we describe the different model experiments that we perform and their relationships to the research questions. Before discussing the specific experiments, we point out that our model consists of a large set of parameters and initial and boundary conditions. Since in most of the experiments these are identical, we summarise them in Table I. In this section we discuss only the specific characteristics of each experiment.

In the first experiment, we evaluate our derived equilibrium EF (Equation (6)) against the actual time-varying EF as calculated in an idealized situation in order to determine if, and on which time-scale, equilibrium can be achieved. This situation is initialized from an initial profile that consists only of a constant lapse rate (Figure 2) and is forced with a constant net radiation Q_* of $400\,W\,m^{-2}$.

Table II shows the specifications of the six runs. The integration time is 120 hours. We vary the lapse rate of specific humidity, which has a large influence on Δq, and the initial potential temperature near the surface θ_0 in order to perform a sensitivity analysis on the variables that determine the equilibrium EF (Equation (6)).

From these idealized cases, we proceed to simulations characterized by a semi-diurnal sinusoidal evolution of the net radiation Q_* (from 0600 to 1800 local time (LT), having a maximum of $400\,W\,m^{-1}$ at 1200 LT)

DOI: 10.1002/qj

Table I. Model constants, boundary conditions and initial conditions of coupled model runs. Deviations from this set-up are described in the text. Variables subjected to a sensitivity analysis are indicated by SA.

Parameter	Value	Units	Description
Constants			
A_{θ_v}	SA	–	entrainment/surface ratio buoyancy flux
c_p	1005	$\mathrm{J\,kg^{-1}K^{-1}}$	specific heat of dry air
g	9.81	$\mathrm{m\,s^{-2}}$	gravity acceleration
L_v	2.45×10^6	$\mathrm{J\,kg^{-1}}$	heat of vaporization
R_d	287.05	$\mathrm{J\,kg^{-1}K^{-1}}$	gas constant for dry air
R_v	461.5	$\mathrm{J\,kg^{-1}K^{-1}}$	gas constant for moist air
Boundary conditions			
G	0.1	–	ratio ground heat flux/net radiation
P_0	101300	Pa	surface pressure
$Q_{*\max}$	500	$\mathrm{W\,m^{-2}}$	maximum net radiation
r_s	SA	$\mathrm{s\,m^{-1}}$	stomatal resistance
r_a	50	$\mathrm{s\,m^{-1}}$	aerodynamic resistance
γ_θ	0.005	$\mathrm{K\,m^{-1}}$	free-atmosphere potential temperature lapse rate
γ_q	0.0	$\mathrm{kg\,kg^{-1}m^{-1}}$	free-atmosphere specific humidity lapse rate
Initial conditions			
h_0	100	m	initial CBL height
q_0	$= 0.7q_{\mathrm{sat}}(\theta_0)$	$\mathrm{kg\,kg^{-1}}$	initial mixed-layer specific humidity
Δq_0	SA	$\mathrm{kg\,kg^{-1}}$	initial specific humidity jump at h
θ_0	SA	K	initial mixed-layer potential temperature
$\Delta\theta_0$	4.0	K	initial potential temperature jump at h
θ_{s0}	$= \theta_0$	K	surface potential temperature

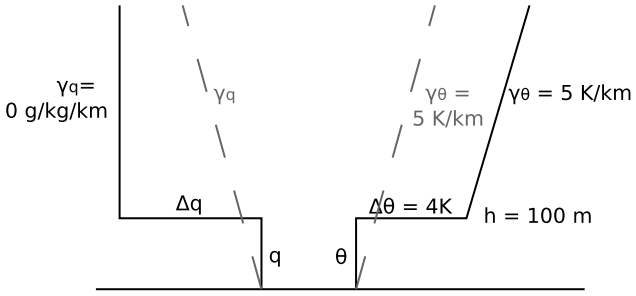

Figure 2. Sketch of initial profiles of specific humidity q and potential temperature θ for idealized cases (grey) and realistic cases (black). Variables θ, q, γ_q and Δq are subjected to a sensitivity analysis during the experiments.

and realistic initial profiles. These profiles are inspired by typical early summer conditions for Cabauw (The Netherlands), shown using the black lines in Figure 2. Although all our model runs are based on real-data-inspired values, we explicitly chose in this study not to do data analysis as this would have limited the possibilities for addressing the effects of dry-air entrainment in a very general way.

In the second experiment (Table III) we analyse the convergence of EF to equilibrium on a semi-diurnal time-scale. Here, we perform our analyses on both wet ($r_s = 0\,\mathrm{s\,m^{-1}}$) and dry ($r_s = 100\,\mathrm{s\,m^{-1}}$) surfaces. The latter merits some attention as Raupach (2001) showed that over dry surfaces the semi-diurnal time-scale is too short to achieve equilibrium. In these experiments we

Table II. Initial mixed-layer potential temperature θ_o and the lapse rate of specific humidity γ_q for the idealized cases.

Run	θ_0 (K)	γ_q ($\mathrm{g\,kg^{-1}km^{-1}}$)
*const*1	285	0
*const*2	285	−3
*const*3	285	−6

Table III. Initial jump of specific humidity at the interface Δq_0, the stomatal resistance of the vegetation r_s and the atmospheric resistance r_a, as used in the realistic experiments.

Run	Δq_0 ($\mathrm{g\,kg^{-1}}$)	r_s ($\mathrm{s\,m^{-1}}$)	r_a ($\mathrm{s\,m^{-1}}$)
*wet*1	0	0	50
*wet*2	−2.5	0	50
*wet*3	−5	0	50
*dry*1	0	100	50
*dry*2	−2.5	100	50
*dry*3	−5	100	50
*wet*1*ra*5	0	0	5
*wet*2*ra*5	−2.5	0	5
*wet*3*ra*5	−5	0	5

DOI: 10.1002/qj

Table IV. Initial mixed-layer potential temperature θ_0, initial jump of specific humidity at the interface Δq_0, stomatal resistance of the vegetation r_s and entrainment coefficient A_{θ_v} for series of runs performed.

Series	Δq_0 (g kg^{-1})	θ_0 (K)	r_s (s m^{-1})	A_{θ_v}
$seriesrs0$	$-4-0$	$275-295$	0	0.2
$seriesrs50$	$-4-0$	$275-295$	50	0.2
$seriesrs100$	$-4-0$	$275-295$	100	0.2
$seriesA_{\theta_v}$	$-4-0$	280	50	$0.05-0.6$
$seriesT290$	$-4-0$	290	$0-400$	0.2

chose to fix the initial potential temperature at 285 K and to vary the initial Δq_0 and the surface resistance r_s. Notice that the first six runs have realistic values for the aerodynamic resistance r_a and that three additional runs with a very small value of 5 s m^{-1} for r_a are included, in order to enable us to discuss the relevance of r_a to the convergence of the EF to equilibrium.

Following our analysis of the equilibrium EF on a semi-diurnal time-scale, we continue by illustrating the effect of land–atmosphere coupling for cases $dry1$, $dry2$ and $dry3$ from the previous experiment. In a comparison of the temporal evolution of the three cases, we explore the effect of dry-air entrainment on the surface heat fluxes, on the CBL height and the potential temperature and the specific humidity of the CBL.

In the final experiment, we perform an extensive sensitivity analysis that consists of series of model runs (Table IV), in order to address the question under which atmospheric and land-surface conditions dry-air entrainment is relevant to the surface fluxes and CBL development. In each series, a sensitivity analysis is performed on two initial or boundary conditions. For each condition a range of 16 values is selected and the model is run for all combinations. All experiments start at 0600 LT and last until 1300 LT. The model results at 1300 LT are stored and used for the analyses. First, we investigate the sensitivity of dry-air entrainment to initial temperature over a well-watered soil ($seriesrs50$), a wet soil ($seriesrs0$) and a dry soil ($seriesrs100$) and complete this analysis by evaluating the sensitivity of the results to the value of the entrainment coefficient ($seriesA_{\theta_v}$). For the analysis, we create contour plots of the EF, CBL height and RH at the land surface and the CBL top at 1300 LT. Second, in $seriesT290$ we evaluated the importance of the free-tropospheric moisture conditions against the land-surface properties by varying the initial specific humidity jump, Δq, and the stomatal resistance, r_s.

4. Results

4.1. Idealised validation of derived equilibrium EF

In the first experiment, we look at whether our coupled land–atmosphere system converges to the previously defined equilibrium expression for the evaporative fraction (Equation (6)). The experiment consists of a set of model runs (Table II), the results of which are shown in Figure 3.

The figure validates our derived equilibrium expression by showing that the three cases with constant forcings converge to equilibrium. If we define equilibrium as the state in which the EF is within 2% of the equilibrium EF, then *const1* reaches equilibrium after 45 hours at an EF of 0.81, *const2* after 19 hours with $EF = 0.86$, and *const3* (which has the largest dry-air entrainment) after 10 hours at an EF of 0.91. In addition to confirming the convergence of the system to equilibrium, the results also reveal information about the magnitude and the characteristic time-scale of the convergence to equilibrium. Dry-air entrainment enhances the equilibrium EF, but at the same time it tends to greatly decrease the characteristic time-scale of the system, as was shown by Raupach (2000). The enhancement is explained by Equation (6), as a larger negative value for Δq results in a larger value for the equilibrium EF, because dry air supports larger evaporation rates. The more rapid convergence to equilibrium can be attributed to an increase of the efficiency of the drying feedback (Figure 1). When the free troposphere is dry, an increase in CBL height results in a larger reduction in q in the CBL by the entrainment of dry free-tropospheric air, compared to conditions with a moist free troposphere. In section 4.3, we discuss this feedback mechanism in more detail.

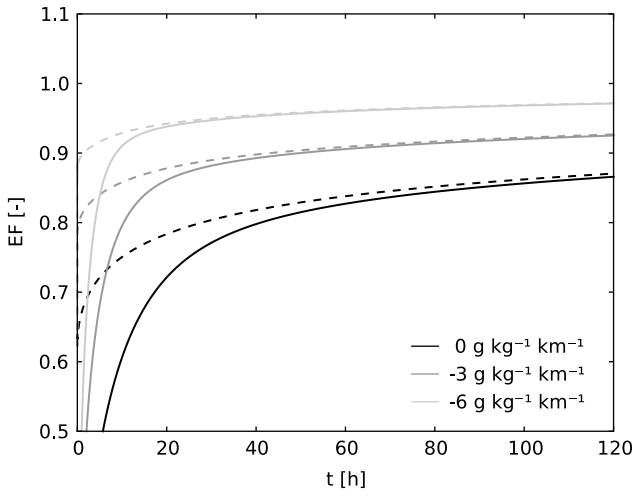

Figure 3. Evaporative fraction (solid lines) and equilibrium EF (dashed lines, calculated from model data using Equation (6)) as a function of time in cases *const1*, *const2* and *const3* (Table II).

DOI: 10.1002/qj

4.2. Validation of equilibrium EF on a semi-diurnal time-scale

This experiment evaluates the applicability of equilibrium evaporation on a semi-diurnal time-scale (Figure 4).

The cases with a diurnal cycle of net radiation (Figure 4(a)) show that between 1200 and 1400 LT the EF approximates equilibrium evaporation. As in the idealised cases, entrainment enhances the EF throughout the whole day. At 1300 LT the values of the EF of cases *wet1*, *wet2* and *wet3* are 0.89, 0.95 and 0.99 respectively, while the equilibria for the same cases are 0.89, 0.94 and 0.98. In contrast to the cases with constant surface forcings, the convergence to equilibrium is less evident.

Although the EF follows the equilibrium with a time lag close to one hour, there is never convergence, because the forcings change more rapidly than the adjustment time of the equilibrium EF. In other words, the characteristic time-scale of the feedbacks is too long, because the atmospheric resistance r_a is fixed at $50\,\mathrm{s\,m^{-1}}$ under our conditions. If we set the resistance to a very low value (Figure 4(b)) of $5\,\mathrm{s\,m^{-1}}$, allowing the atmosphere to take up water very quickly, we drastically reduce the characteristic time-scale of the feedbacks. Under these conditions, convergence for this case is clearly visible from the figure, thereby proving that during the day the systems still tend to converge to equilibrium. In this special limiting case, the EF reaches values larger than 1. Despite the slightly negative sensible heat flux in such situations, the virtual potential flux is still positive due to the large moisture flux. Therefore, convection is maintained and our model is still valid.

In spite of the fact that, under the conditions of our numerical experiments, convergence is not achieved during the day, the equilibrium EF is still an appropriate indicator of the effect of dry-air entrainment. The enhancement of the equilibrium EF from $wet1$ to $wet3$ corresponds well to the enhancement found in the actual EF for those cases. In Figure 5 we plotted the semi-diurnal evolution of EF for the cases with a dry soil ($r_s = 100\,\mathrm{s\,m^{-1}}$).

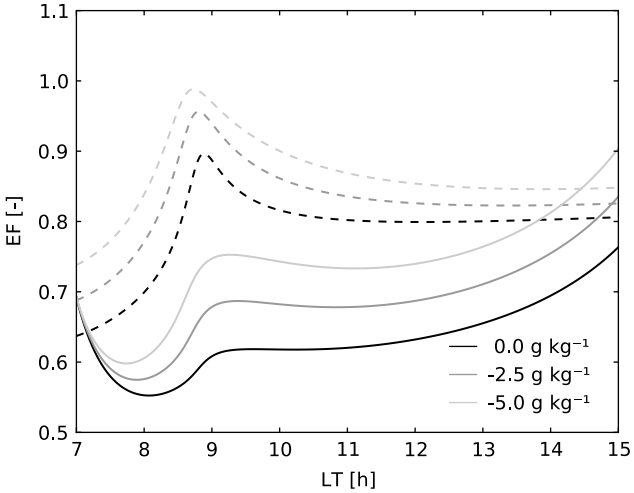

Figure 5. Evaporative fraction (solid lines) and equilibrium EF (dashed lines, calculated from model data using Equation (6)) as a function of time in cases *dry1*, *dry2* and *dry3* (see Table III).

The importance of dry-air entrainment is very pronounced in the EF, even though its values are now far from equilibrium. For instance, case $dry1$ has an EF of 0.66 at 1300 LT and $dry3$ of 0.76, which is the same enhancement of 0.10 by dry-air entrainment as is found in the wet cases discussed above. Our results thus extend the findings of de Bruin (1983) to dry surfaces. Here, we found enhancements of evaporation by dry-air entrainment over dry soils that equal the enhancements over wet soils. We would stress that, even over dry soils, the increase in the equilibrium EF is a good indicator of the increase in the actual EF. For this reason, the change in the evaporation induced by a modification in the free-tropospheric properties can be estimated by using the simple expression for equilibrium (Equation (6)).

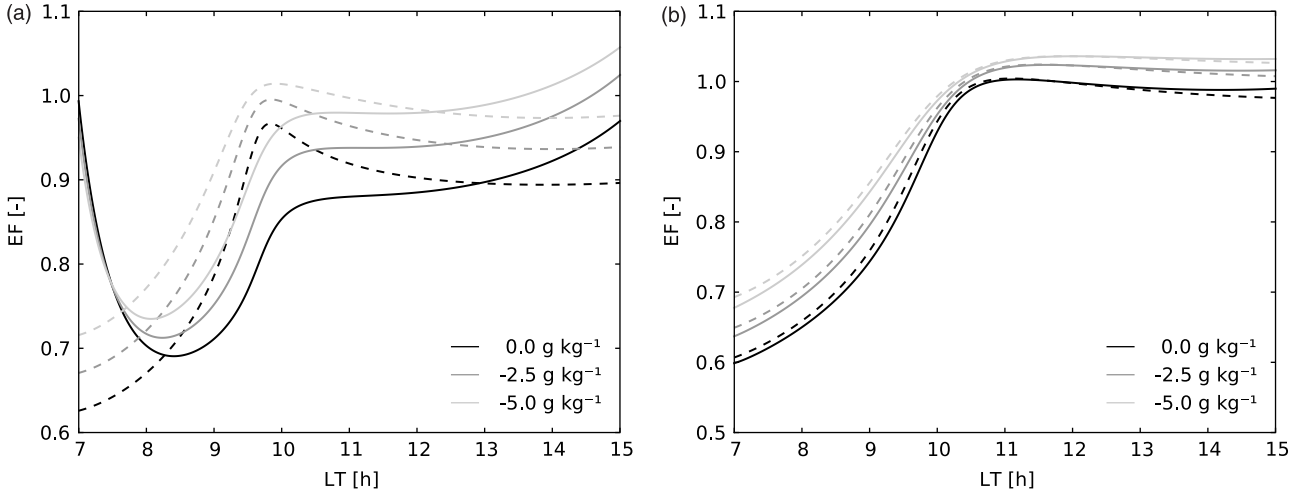

Figure 4. (a) Evaporative fraction (solid lines) and equilibrium EF (dashed lines, calculated using equation 6) as a function of time in cases *wet1*, *wet2* and *wet3*. (b) Time evolution of EF and equilibrium EF of *wet1ra5*, *wet2ra5* and *wet3ra5* (see Table III).

DOI: 10.1002/qj

4.3. Dry-air entrainment and land–atmosphere coupling

The results of the previous experiments showed us that dry-air entrainment clearly enhances surface evaporation. In this section we further analyse the consequences of the enhancement for the CBL properties. We select case *dry1*, *dry2* and *dry3* to serve as example cases to determine the effect of all the feedbacks, before discussing the general and less specific approach of our final experiment.

Figure 6 shows the temporal evolution of the CBL variables that are involved in the feedback loops (Figure 1). It is obvious that evaporation is enhanced by dry-air entrainment (Figure 6(a)). For instance, at 1200 LT *dry1* has a LE of 228 W m^{-2} and *dry3*, with the largest dry-air entrainment, has 268 W m^{-2}. This is a moderate increase of 40 W m^{-2}, but with significant implications for other variables. The effects of dry-air entrainment are most profound when the CBL grows most rapidly, between 0830 and 1000 LT. During this period large amounts of dry air enter the CBL, as is made evident by the rapid drop in specific humidity (Figure 6(c)). The reduction is particularly large in *dry3*, where q drops to 2.4 g kg^{-1} at 1200 LT, compared to 6.3 g kg^{-1} for *dry1*. In this case, the stronger drying feedback (Figure 1) enhances evaporation moderately, but induces a strong relative reduction in the sensible heat flux. At 1200 LT the sensible heat flux has fallen by 29% (from 132 to 94 W m^{-2}). As CBL growth is driven by H, the modification of the surface fluxes by dry-air entrainment is evident in the time evolution of this variable. Dry-air entrainment reduces the CBL height at 1500 LT from 1165 m to 1007 m. This has significant effects on the RH at the top of the CBL and thus on cloud formation, which we discuss in our analyses of the final experiment.

In spite of the large entrainment-induced changes in CBL height and specific humidity, the temperature is less sensitive to dry-air entrainment, although the surface sensible heat flux has fallen significantly. The reason for this is that the largest heating occurs while the CBL is hardly growing (between 0700 and 1000 LT) and at that time the three cases still have nearly identical CBL properties. In addition, the contribution of heat entrainment to the total temperature tendency is relatively small compared to the contribution of dry-air entrainment to the tendency of specific humidity. Nevertheless, the dry-air entrainment-induced temperature change is 0.9 K at 1500 LT.

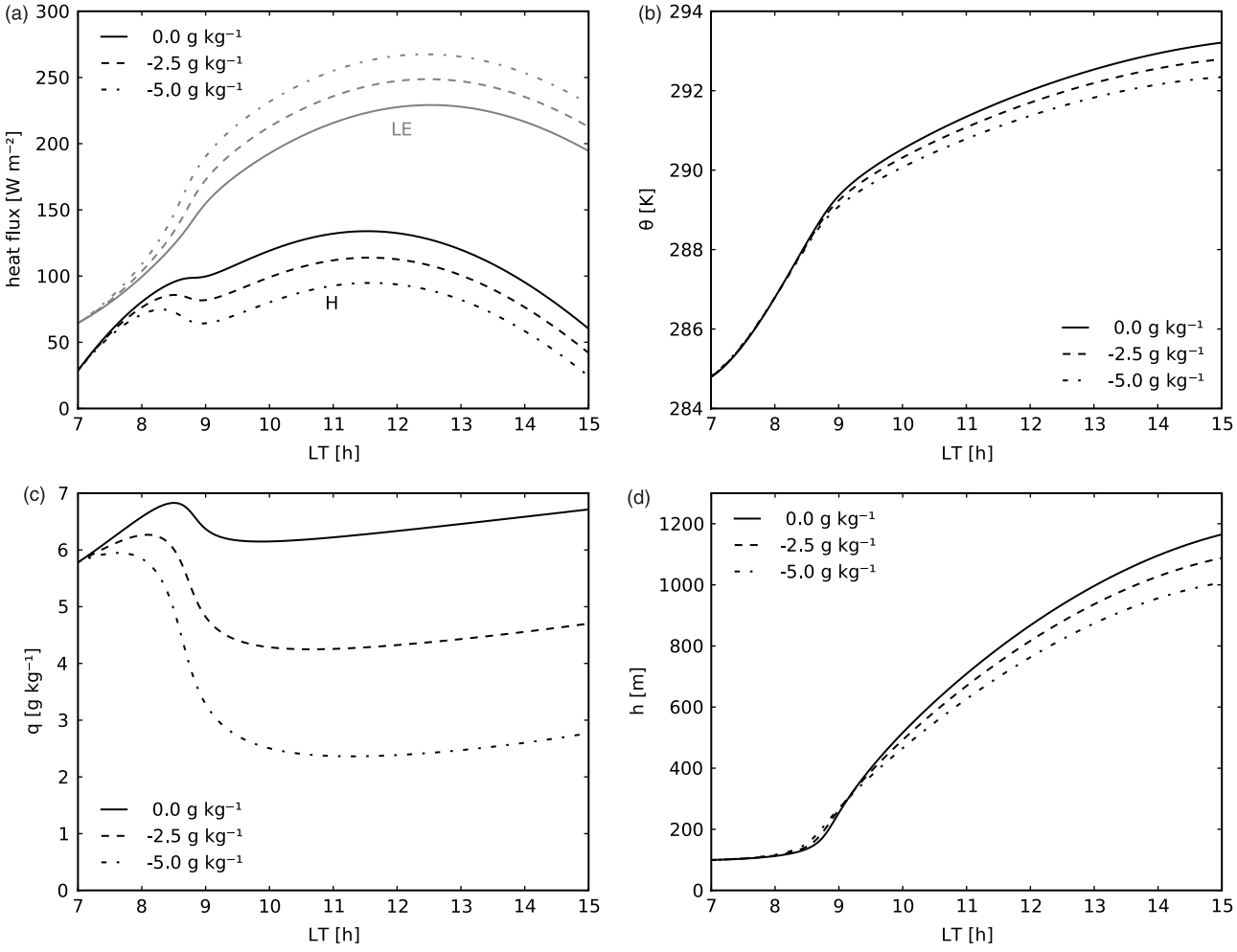

Figure 6. Time series of surface heat fluxes and CBL variables in cases *dry1*, *dry2* and *dry3* (Table III). (a) shows the surface heat fluxes, (b) the CBL potential temperature, (c) the specific humidity of the CBL, and (d) the CBL height.

DOI: 10.1002/qj

4.4. The impacts of dry-air entrainment on surface heat fluxes and CBL development in a wide range of conditions

To summarise the results so far, we found that dry-air entrainment significantly enhances the equilibrium evaporation. This in turn influences the development of the CBL and the possible occurence of clouds. In the following experiment we evaluate the effects of dry-air entrainment in a large parameter space to investigate its sensitivity to the atmospheric and land-surface conditions.

4.4.1. The influence on evaporation and near-surface RH

We start the experiment by investigating the role played by atmospheric conditions. For this purpose, we perform *seriesrs*50 in which we vary the initial values for the potential temperature and the jump of specific humidity between the CBL and the free troposphere. These variables are selected, because they determine the value of the equilibrium EF (Equation (6)) and the relative contribution of each of the feedback mechanisms involved (Figure 1). Figure 7(a) shows the values of the EF and the Priestley–Taylor parameter at 1300 LT as a function of these variables.

It is clear that the EF at 1300 LT is larger if the free troposphere is drier, regardless of the initial potential temperatures. For instance, at an initial temperature of 275 K the EF is 0.53 for an initial $\Delta q_0 = 0.0\,\mathrm{g\,kg^{-1}}$, while it rises to 0.70 at $\Delta q_0 = -4.0\,\mathrm{g\,kg^{-1}}$. Furthermore, the EF increases with increasing temperature for all Δq_0. Although initial potential temperature and initial specific humidity are both unambiguously correlated with the EF, we find that the sensitivity of EF to the initial Δq_0 becomes less at higher temperatures. Equation (6) explains that the equilibrium evaporation increases with temperature, due to the exponential character of the saturated specific humidity curve. The EF therefore increases at higher temperatures. The drying feedback therefore has less influence, because of the lower availability of energy for the sensible heat flux. This explains the lower sensitivity of EF for Δq_0.

The values of the Priestley–Taylor parameter α (Figure 7) also show a dependence on the initial Δq. Dry-air entrainment enhances the α value, but at high temperatures the sensitivity is low. For a wide range of conditions, we model values for α close to the 1.26 that Priestley and Taylor (1972) found for well-watered surfaces. Since dry-air entrainment is the only possible reason for enhanced evaporation in our model, we attribute the larger than unity value of α to this phenomenon.

Figure 7(b) shows the RH at the land surface for the same range of initial conditions as Figure 7(a). The EF is contoured in black as a reference. Like the EF, the RH is also sensitive to the initial Δq at low temperatures and is less sensitive at high temperatures. We find a poor correlation between evaporation and RH at the land surface, which has also been observed by Juang *et al.* (2007) and Siqueira *et al.* (2009). This is because the increase in evaporation achieved through the drying feedback has the opposite influence on RH as the heating feedback. For instance, if we move in the figure to larger values of EF parallel to the initial temperature axis, we find a rise of RH because of the increase in EF due to higher temperatures. However, if we enhance evaporation through an increase of dry-air entrainment, the figure shows a decrease of the RH, because of the drier air. There is therefore a range of combinations of initial potential temperatures and specific humidities that produce the same value for EF at 1300 LT, but significantly different values for RH.

We repeated the whole analysis in this section also for wet surfaces in *seriesrs*0 and for dry surfaces in *seriesrs*100 (not shown). Here, similar behaviour was found as in *seriesrs*50, except that the EF and RH have higher values under all the initial conditions in *seriesrs*0 and lower values in *seriesrs*100. This is due to the fact that the land surface can meet the atmospheric demand

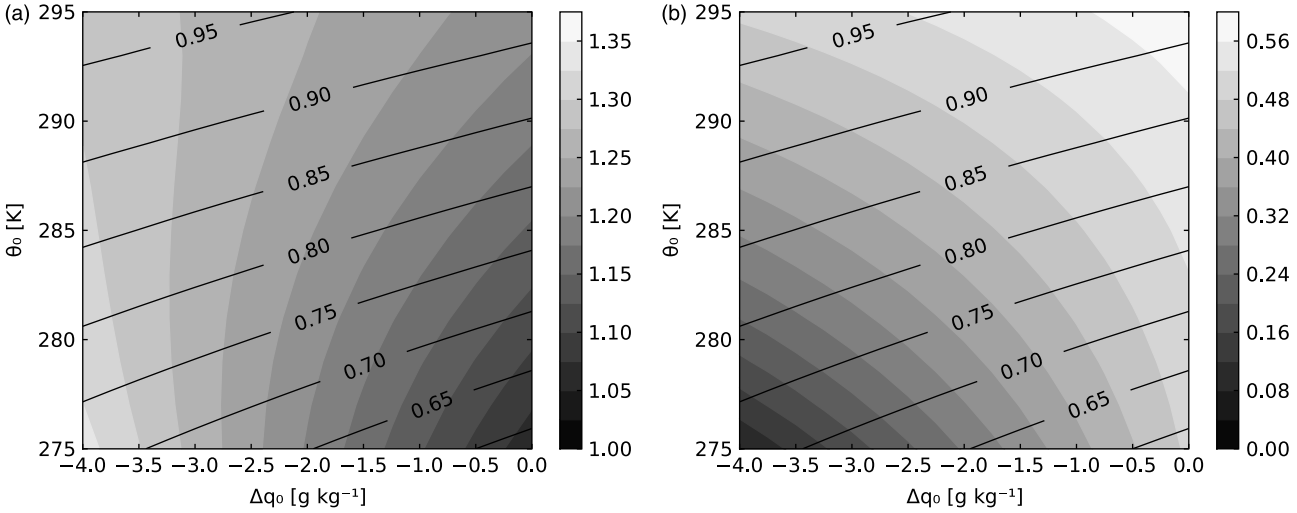

Figure 7. (a) evaporative fraction (contours) and the Priestley-Taylor parameter α (shading) at 1300 LT as a function of the initial specific humidity jump Δq_0 and the initial potential temperature θ_0. (b) relative humidity at the land surface (shading) and the evaporative fraction (contours). Both panels are based on the results of *seriesrs50*.

DOI: 10.1002/qj

for water more rapidly when the surface is wet and slower when the surface is dry.

4.4.2. *The influence on the conditions at the CBL top*

So far, we have found that dry-air entrainment under all conditions influences the surface heat fluxes. Since these effects are to a large extent a function of temperature, the modification of the CBL properties by entrainment must also be temperature dependent. Figure 8 shows the influence of dry-air entrainment on CBL height and RH at the top of the CBL for *seriesrs50* at 1300 LT.

In Figure 8(a), the CBL height decreases as the initial Δq_0 becomes more negative. This is explained by the fact that dry-air entrainment enhances the equilibrium EF (see previous section). For this reason, the LE increases and the subsequent reduction in the sensible heat flux results in a lower CBL. For instance, at 280 K the height of the CBL for a Δq_0 of zero is 1100 m, while in a dry atmosphere ($\Delta q_0 = -4.0\,\mathrm{g\,kg^{-1}}$) the CBL height is only 950 m. Moreover, as temperature increases, the CBL height displays straightforward behaviour. Under all free-tropospheric moisture conditions, an increase of 1 K results in a CBL that is about 22 m less deep.

In spite of the simple relationship between the CBL height and the initial conditions, the RH at the CBL top (RHtop) is nonlinear. The RHtop decreases if Δq_0 becomes more negative for all initial temperatures. In addition, the sensitivity of RHtop to Δq_0 is much larger at low temperatures than at high temperatures, due to the importance of the drying feedback under these conditions. We already have discussed this in detail in the previous section.

However, the response of the RH at the CBL top to initial temperature changes is complex. If the free troposphere is moist, the RHtop falls as temperature rises. At a $\Delta q_0 = -0.5\,\mathrm{g\,kg^{-1}}$, the RHtop drops from 0.95 to 0.87 in the temperature range from 275 to 295 K. However, under conditions of a dry free troposphere, for instance at $\Delta q_0 = -3.0\,\mathrm{g\,kg^{-1}}$, the RHtop increases from 0.45 to 0.76 over the same temperature range. To explain the difference between these two situations, it is important to define the role of the different competing processes in the determination of RH. The evolution of RHtop is the result of competition between RH-enhancing processes, such as surface evaporation and absolute temperature decrease by CBL growth, with RH-reducing processes, such as dry-air entrainment and CBL heating (Ek and Mahrt, 1994; Ek and Holtslag, 2004). Our feedback diagram (Figure 1) may help us to understand the effects of rising temperature. An increase in temperature enhances evaporation through the heating feedback. Energy is thus shifted towards the latent heat flux, thereby decreasing the sensible heat flux. In consequence, there is less CBL growth and less free-tropospheric air is therefore entrained into the CBL. In the case of a dry free troposphere, this produces an increase of the RH, because the increase in RHtop due to less dry-air entrainment is the most essential process. However, beneath a moist free troposphere the drying effect of entrainment is not important. The increase of absolute temperature at the top of the CBL, as a consequency of the decrease in boundary-layer height, thus results in a lowered RH.

Figure 8(b) shows the evaporative fraction, but this time combined with the CBL height. We have already discussed the behaviour of the two quantities, but it is important to note that the two are highly correlated. The EF determines which fraction of the energy is available for the sensible heat flux, which is the driving force of boundary-layer growth. Therefore, cases that share the same EF should have approximately the same CBL height. If we analyze the figure carefuly, we find that the EF is more sensitive to initial Δq_0 than the CBL height. This is because all cases initially have the same CBL height and the same EF despite their different initial Δq_0 value. During the period of fast CBL growth, differences between the cases start to develop (see also

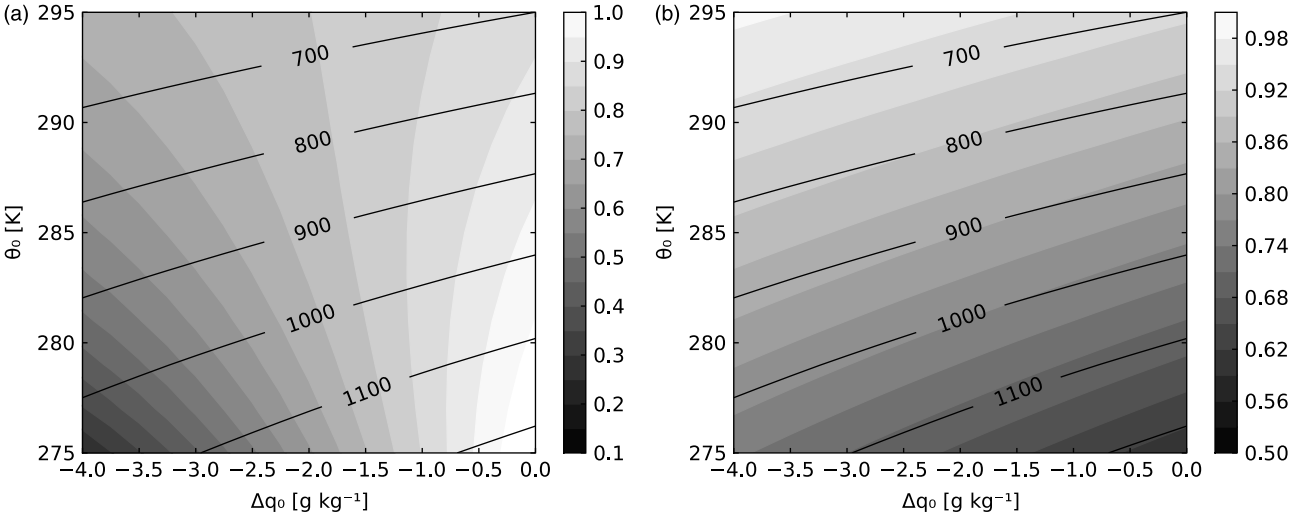

Figure 8. (a) relative humidity at the CBL top (shading) and the CBL height (contours) at 1300 LT as a function of the initial specific humidity jump Δq_0 and the initial potential temperature θ_0. (b) evaporative fraction (shading) and the CBL height (contours) at 1300 LT. Both panels are based on the results of *seriesrs50*.

DOI: 10.1002/qj

the development of h and q in Figure 6). The CBL height is the integrated result of the sensible heat fluxes during the whole period until 1300 LT, while the EF corresponds to the actual surface fluxes at that time. Therefore, the evolution of CBL height is less sensitive than EF moving over the initial Δq_0 axis because the integrated heat fluxes between the cases are less different than the actual heat fluxes at 1300 LT.

So far, the results have shown a large impact of dry-air entrainment on the surface fluxes and the CBL height. In our model the entrainment of virtual potential temperature, the driving force for CBL growth, is parametrized by Equation (4). Therefore, the value of A_{θ_v} has, according to Equation (6), a significant impact on the equilibruim evaporation. In Figure 9 we evaluate therefore the sensitivity of the EF and the CBL height to the initial specific humidity and the entrainment parameter A_{θ_v}.

The figure shows that larger values for A_{θ_v}, thus more entrainment, lead to higher boundary layers in all conditions. Doubling A_{θ_v} from 0.2 to 0.4 results in a CBL that is approximately 100 m higher. However, the effects on EF are only marginal, since a doubling of A_{θ_v} results here in enhancements of only approximately 0.01 in all conditions. This implies that, despite the larger CBL growth, an increase in A_{θ_v} leads to only little enhancement of the drying feedback. The reason is that during the rapid growth phase of the CBL, the specific humidity quickly drops (Figure 6), thereby approaching the free-tropospheric value. In such conditions, a larger A_{θ_v} does increase the CBL growth, but not the dry-air entrainment since Δq has a very small value. Therefore, the influence of dry-air entrainment on the surface heat fluxes is much more dependent on the initial Δq than on the entrainment parameter A_{θ_v}.

It is interesting and relevant to link the implications of our model results to convective cloud formation. In the case of constant land-surface conditions, a reduction of the free-tropospheric moisture results in a decrease of the RHtop and cloud formation therefore reduces or initiates later in the day. An increase in early morning temperature can result in more cloud formation in a dry free atmosphere or to less cloud formation in a moist situation. Our study provides a framework for the analyis of case-studies such as that of Vilà-Guerau de Arellano (2007).

4.4.3. *Importance of land-surface properties versus free troposphere conditions*

Previous studies (e.g. de Bruin, 1983; Santanello *et al.*, 2007; Trier *et al.*, 2008) have treated the land surface as the fundamental determinator of the partitioning of the surface heat fluxes. In order to compare the relative importance of land surface to free-tropospheric moisture conditions, we perform *seriesT290*, a series of trials with a range of surface resistances and initial specific humidity jumps.

Figure 10(a) shows RH and EF as functions of the initial specific humidity (Δq_0) and of the land-surface resistance r_s, which for grassland can be regarded as

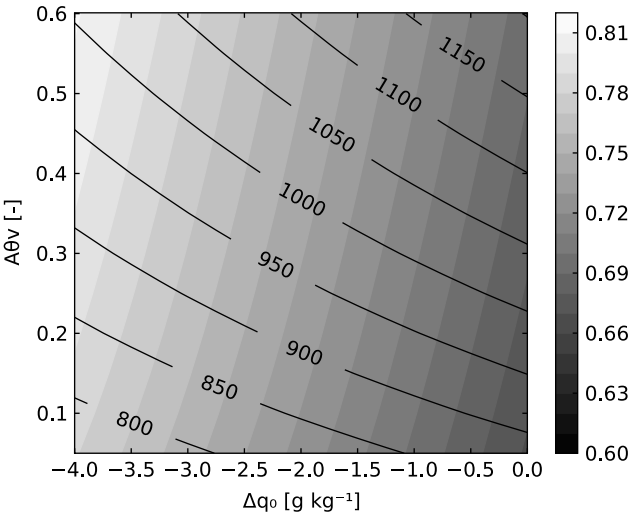

Figure 9. Evaporative fraction (shading) and the CBL height (contours) at 1300 LT as a function of the initial specific humidity jump Δq_0 and the entrainment parameter A_{θ_v}, based on the results of *series*A_{θ_v}.

a measure of the water availability of the soil. The figure shows that over all surface resistances, dry-air entrainment produces an increase in EF and a fall in RH, as we have already explained in the discussion of Figure 7. This figure also shows that an increase in the surface resistance r_s results in a decrease of EF and RH. However, the reduction in EF is not the effect of a reduction in equilibrium evaporation, but rather of an increase in the characteristic time-scale of the coupled system under dry conditions. Figures 4 and 5 show that in all cases the equilibrium EF is low in the early morning due to the low temperature and the relatively high specific humidity in the CBL (Figure 6). Subsequently, after sunrise the forcings rapidly increase the equilibrium EF. However, in the dry cases (large r_s) in the upper parts of Figure 10, the system adapts only slowly to a larger equilibrium EF, as we learned from Figure 5. The EF therefore remains low, due to the characteristic long time-scale of the coupled system under dry conditions (Raupach, 2000, 2001). In consequence, the CBL heats and grows rapidly, resulting in a low RH. The figure also shows that the sensitivity of the RH to dry-air entrainment rises if r_s increases. This is because, in spite of the overall low strength of the feedbacks, the drying feedback still increases in line with the sensible heat flux. At high resistances we have a large sensible heat flux, with the result that the dry-air entrainment reduces the RH more than under conditions with a low sensible heat flux.

We show the CBL height and the RH at the top of the CBL in Figure 10(b). The CBL height responds as expected to changes in r_s as a greater resistance and thus more sensible heat results in a higher CBL. The response of CBL height to changes in Δq_0 has already been discussed in Figure 7. We also find that the RH at the top of the CBL decreases for larger negative values of Δq_0. The decrease of RHtop as well as the reduced sensitivity of that variable for large values of r_s can be explained using similar arguments as for the RH findings

DOI: 10.1002/qj

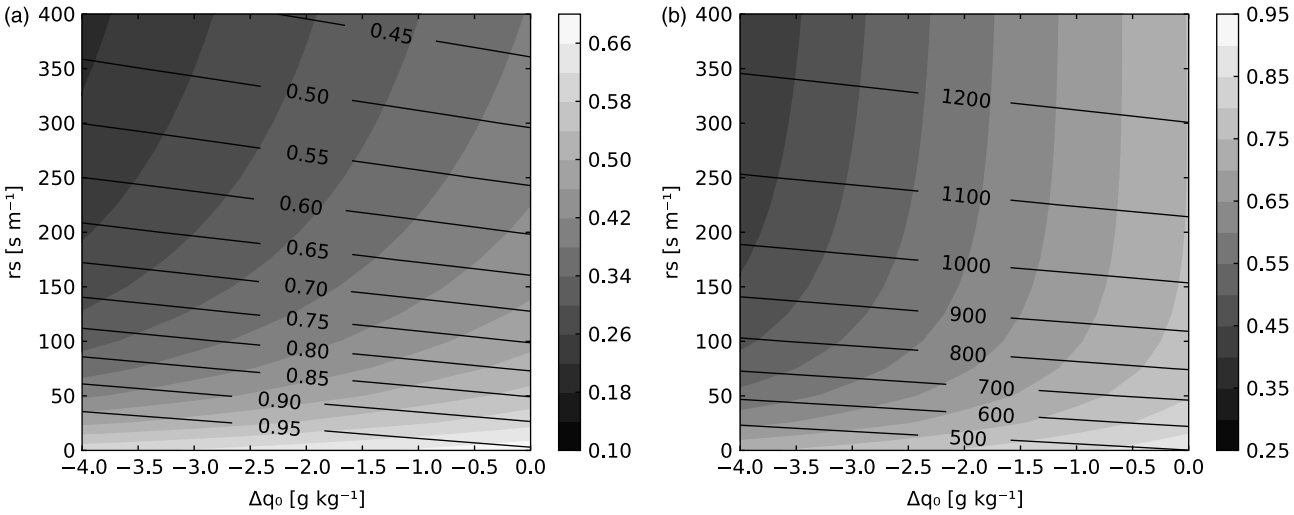

Figure 10. (a) relative humidity at the land surface (shading) and the evaporative fraction (contours) at 1300 LT as a function of the initial specific humidity jump Δq_0 and the surface resistance r_s. (b) relative humidity at the CBL top (shading) and the CBL height (contour lines). Both figures are based on the results of *seriesT290*.

in Figure 10(a). The figure also shows that if we move along the r_s-axis in the direction of larger r_s we find a rapid decrease in RH at low values of r_s. When we move towards large r_s values, the RHtop continues to decrease, but the sensitivity vanishes at high resistances, especially if the free troposphere is moist. Eventually, RHtop becomes constant even while the CBL height continues to increase with r_s. Figure 10(a) shows us that EF also decreases in line with r_s. If the CBL continues to be enhanced for an increasing r_s, thereby increasing the RHtop, then other processes must exactly compensate this effect here. Figure 6 showed that q becomes constant in the afternoon: to maintain the same RHtop, therefore, the absolute temperature at the CBL top must remain constant. To achieve this, the cooling of the absolute temperature at the CBL top by boundary-layer growth is compensated for by warming induced through the surface and the entrainment heat flux.

Our results indicate that, as de Bruin (1983) concluded, r_s is the most sensitive parameter in the determination of surface evaporation. Nevertheless, a decrease in free tropospheric moisture by $4\,\mathrm{g\,kg^{-1}}$, which can happen in a time-scale of hours (Vilà-Guerau de Arellano, 2007), results in an increase in evaporation of 5 to 10%, depending on temperature. It should also be emphasised that land–atmosphere feedbacks make cloud formation insensitive to land-surface properties over very dry surfaces (large r_s). Under such conditions, free-tropospheric specific humidity is the key variable.

5. Conclusions

This study addressed the effects of dry-air entrainment on the surface evaporation and the development of the convective boundary layer (CBL), through associated feedback mechanisms. We used a simple mixed-layer model coupled to the land surface with the Penman–Monteith equation to reproduce the essential physics of the coupled land–atmosphere system.

First, we studied the physical properties of the feedbacks in the coupled land–atmosphere system. This produced a framework that enables us to separate the effects of dry-air entrainment from the other feedbacks in the system. Using this framework, we derived simple equilibrium expressions for the evaporative fraction, EF, and the Priestley–Taylor parameter, α, and showed that the expressions are valid. However, only over wet surfaces is the evaporation able to approach equilibrium on a semi-diurnal time-scale. Nevertheless, over dry land surfaces the expression is still a good indicator of the enhancement of surface evaporation by dry-air entrainment.

Second, we studied the impact of dry-air entrainment on the evolution of the surface fluxes and atmospheric properties throughout the day for a wide range of atmospheric conditions. The most important finding of this study is that dry-air entrainment enhances surface evaporation significantly under all conditions, but to different degrees. More specifically, dry-air entrainment has more influence on the surface heat fluxes at low potential temperatures (275–280 K) than at higher potential temperatures (290–295 K). This is because under cooler conditions the feedback in which dry-air entrainment is contained is the most dominant one. The analysis shows that dry-air entrainment is the process which creates a poor correlation between RH and evaporation at the surface.

By modifying the surface heat fluxes, dry-air entrainment has a major effect on CBL height and RH at the top of the CBL. An increase in evaporation by dry-air entrainment results in a relatively large reduction of the sensible heat flux, as the latent heat flux is normally larger than the sensible heat flux over vegetated surfaces. As this is the driving force of CBL growth, dry-air entrainment potentially reduces the CBL height by hundreds of metres compared to a situation in which the free troposphere contains more moisture. The choice of the value

DOI: 10.1002/qj

of the entrainment parameter A_{θ_v} has only little impact on the surface fluxes, despite its strong influence on the growth of the CBL, because the dry-air entrainment is limited by the moisture difference between the CBL and the free troposphere, rather than by the rate of CBL growth.

The interactions of dry-air entrainment and surface fluxes lead to nonlinear responses of the RH at the CBL top (RHtop). The value of this variable falls if there is more dry-air entrainment. However, the response of RHtop to a rise in initial temperature is nonlinear. A rise in temperature results in a larger EF and thus in a reduced surface sensible heat flux and less CBL growth. In situations characterized by a dry free troposphere, less CBL growth results especially in less drying by entrainment, thus RHtop rises. However, if the free troposphere is moist, then the increase of absolute temperature induced by less CBL growth is stronger than the reduced drying, thus RHtop falls.

Third and last, we compared the relative importance of free-tropospheric moisture conditions with land-surface properties vis-à-vis the values of surface fluxes and CBL properties. The surface resistance, which is related to vegetation and soil moisture, is found to be the most sensitive parameter in the determination of the surface fluxes and the CBL height. However, the free-tropospheric moisture content still has a significant effect on the surface fluxes. Regarding the RH at the CBL top, the effects of free-tropospheric moisture conditions are more important than the effects of land-surface conditions.

Our results thus contain an important message for modellers. To reproduce realistic surface fluxes and CBL properties, it is essential not only to have correct land-surface properties and temperature profiles, but it is also fundamental to have accurate moisture profiles and to represent dry-air entrainment properly. For studies regarding cloud formation, it is essential to understand that dry-air entrainment determines whether a rise in temperature enhances or surpresses cloud formation. If the free troposphere is dry, a temperature rise enhances the possibility of cloud formation, while it reduces this possibility if the free troposphere is moist.

To conclude, our study can serve as a framework for modellers to quickly understand how sensitive their model results are to dry-air entrainment. We recommended to check first whether dry-air entrainment has a significant impact by calculating the Priestley–Taylor parameter α from Equation (9). This calculation requires vertical profiles of temperature and moisture, either from measurements or from model results. If α exceeds unity, then dry-air entrainment is fundamental in the determination of the surface fluxes. In that case, our contour plots serve as an indication of how changes in the surface characteristics or the atmospheric moisture structure influence the surface heat fluxes, the RH and the CBL height. Since our contour plots do not cover all situations (because we prescribed in all simulations the same cycle of net radiation and we fixed either the surface resistance or the initial temperature), we are aiming at extending this work into a more flexible framework in a future paper. In this future research we will incorporate less idealized vertical profiles of temperature and moisture, more detailed radiation, clouds and additional external forcings such as advection and subsidence.

Acknowledgements

The authors acknowledge the helpful comments of Henk de Bruin and three anonymous reviewers. This study was supported by a grant from the Netherlands Organisation for Scientific Research (NWO TopTalent).

References

Betts AK. 1994. Relation between equilibrium evaporation and the saturation pressure budget. *Boundary-layer Meteorol.* **71**: 235–245.
Betts AK. 2004. Understanding hydrometeorology using global models. *Bull. Am. Meteorol. Soc.* **85**: 1673–1688.
Conzemius RJ, Fedorovich E. 2006. Dynamics of sheared convective boundary layer entrainment. Part I: methodological background and large-eddy simulations. *J. Atmos. Sci.* **63**: 1151–1178.
Culf A. 1994. Equilibrium evaporation beneath a growing convective boundary layer. *Boundary-layer Meteorol.* **70**: 37–49.
de Bruin HAR. 1983. A model for the Priestley-Taylor parameter α. *J. Appl. Meteorol.* **32**: 572–578.
de Bruin HAR, Holtslag AAM. 1982. A simple parameterization of the surface fluxes of sensible and latent heat during daytime compared with the Penman–Monteith concept. *J. Appl. Meteorol.* **21**: 1610–1621.
Ek MB, Holtslag AAM. 2004. Influence of soil moisture on boundary-layer cloud development. *J. Hydrometeorol.* **5**: 86–99.
Ek MB, Mahrt L. 1994. Daytime evolution of relative humidity at the boundary-layer top. *Mon. Weather Rev.* **122**: 2709–2721.
Freedman JM, Fitzjarrald RD, Moore KE, Sakai RK. 2001. Boundary-layer clouds and vegetation–atmosphere feedbacks. *J. Climate* **14**: 180–197.
Jacobs CJM, de Bruin HAR. 1992. The sensitivity of regional transpiration to land-surface characteristics: significance of feedback. *J. Climate* **5**: 683–698.
Juang J-Y, Porporato A, Stoy PC, Siquera MS, Oishi AC, Detto M, Kim H-S, Katul G. 2007. Hydrologic and atmospheric controls on initiation of convective precipitation events. *Water Resour. Res.* **43**: W03421. DOI: 10.1029/2006WR004954.
McNaughton KG, Spriggs TW. 1986. A mixed-layer model for regional evaporation. *Boundary-layer Meteorol.* **34**: 243–262.
Monteith JL. 1965. Evaporation and environment. *Sympos. Soc. Exp. Biol.* **19**: 205–224.
Pino D, Vilà-Guerau de Arellano J, Kim S-W. 2006. Representing sheared convective boundary layer by zeroth- and first-order-jump mixed-layer models: Large-eddy simulation verification. *J. Appl. Meteorol.* **45**: 1224–1243.
Priestley CHB, Taylor RJ. 1972. On the assessment of surface heat flux and evaporation using large-scale parameters. *Mon. Weather Rev.* **100**: 81–92.
Raupach MR. 1991. Vegetation-atmosphere interaction in homogeneous and heterogeneous terrain: some implications of mixed-layer dynamics. *Plant Ecology* **91**: 105–120. DOI: 10.1007/BF00036051.
Raupach MR. 2000. Equilibrium evaporation and the convective boundary layer. *Boundary-layer Meteorol.* **96**: 107–141.
Raupach MR. 2001. Combination theory and equilibrium evaporation. *Q. J. R. Meteorol. Soc.* **127**: 1149–1181.
Santanello JA, Friedl MA, Ek MB. 2007. Convective planetary boundary-layer interactions with the land surface at diurnal time scales: Diagnostics and feedbacks. *J. Hydrometeorol.* **8**: 1082–1097.
Siqueira M, Katul G, Porporato A. 2009. Soil moisture feedbacks on convection triggers: the role of soil-plant hydrodynamics. *J. Hydrometeorol.* **10**: 96–112.
Sullivan PP, Moeng CH, Stevens B, Lenschow D, Mayor SD. 1998. Structure of the entrainment zone capping the convective atmospheric boundary layer. *J. Atmos. Sci.* **55**: 3042–3064.
Tennekes H. 1973. A model for the dynamics of the inversion above a convective boundary layer. *J. Atmos. Sci.* **30**: 558–567.

Tennekes H. 1981. Basic entrainment equations for the atmospheric boundary layer. *Boundary-layer Meteorol.* **20**: 515–531.
Trier SB, Chen F, Manning KW, LeMone MA, Davis CA. 2008. Sensitivity of the PBL and precipitation in 12-day simulations of warm-season convection using different land surface models and soil wetness conditions. *Mon. Weather Rev.* **136**: 2321–2343.
vanZanten MC, Duynkerke PG, Cuijpers JWM. 1999. Entrainment parameterization in convective boundary layers. *J. Atmos. Sci.* **56**: 813–828.
Vilà-Guerau de Arellano J. 2007. Role of nocturnal turbulence and advection in the formation of shallow cumulus over land. *Q. J. R. Meteorol. Soc.* **133**: 1615–1627.

DOI: 10.1002/qj